THE JOURNAL OF PHYSICAL CHEMISTRY C
A JOURNAL OF THE AMERICAN CHEMICAL SOCIETY

pubs.acs.org/JPCC

Article

Understanding the Role of Rare Earths in Zeolite Y on the Removal of Sulfur from Hydrocarbon Fuels

Kevin X. Lee, Tyler B. Crowl, Henry J. Sokol, M. Daniela Morales-Acosta, and Julia A. Valla*

Cite This: J. Phys. Chem. C 2021, 125, 9107–9118

Read Online

ACCESS | Metrics & More | Article Recommendations | Supporting Information

ABSTRACT: Adsorptive desulfurization is a promising alternative to hydrodesulfurization for minimizing harmful sulfur emissions from hydrocarbon fuels. Cu in Y zeolite (CuY) has shown effective sulfur adsorption, especially when paired with Ce (CuCeY). This study explores other rare earths (REs), including La, Sm, and Nd, in RE and CuRE Y and mesoporous Y (SAY) zeolites for the adsorption of benzothiophene (BT) and dibenzothiophene (DBT). Metal loadings on the zeolites were quantified by using inductively coupled plasma optic emission spectroscopy (ICP-EOS) and X-ray fluorescence (XRF). Characteristic adsorption modes, such as σ-bonding and π-complexation, were observed by using Fourier-transform infrared spectroscopy (FTIR). X-ray diffraction (XRD) Rietveld refinement determined that RE ions prefer the sodalite cages of Y zeolite, while Cu occupies supercage sites. Ce showed the strongest synergy with Cu compared to the other REs and the highest adsorption capacity. The results of this study provide insight into the role of RE exchanged Y on sulfur adsorption.

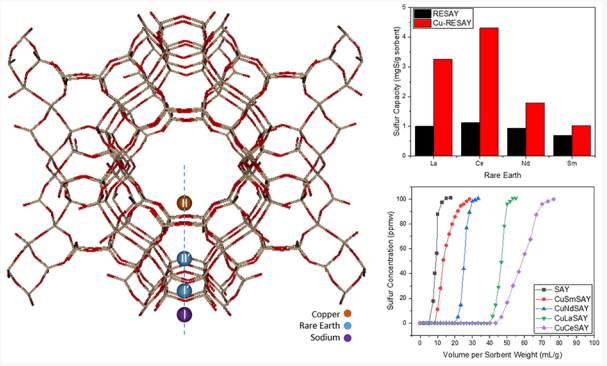

1. INTRODUCTION

The transportation sector in the United States (US) relies heavily on the processing of fossil fuels which produces a plethora of emissions. One of the main components of emissions is sulfur dioxide (SO_2), formed from the combustion of sulfur compounds found naturally in crude oil. SO_2 is detrimental to the integrity of catalytic converters and consequently to the environment, as a precursor to acid rain, and to human health, as an air pollutant. For this reason, the Environmental Protection Agency (EPA) has restricted the sulfur levels of federal gasoline and diesel to be 10 and 15 ppmw, respectively.[1] Sulfur is traditionally removed from crude oil via hydrodesulfurization (HDS), which is successful at removing sulfides, disulfides, and mercaptans, but has difficulty removing larger aromatic sulfur compounds found in diesel and jet fuel.[2] However, HDS cannot attain low levels of sulfur without the use of extreme operating conditions and extensive hydrogen consumption that can degrade the quality of the fuel.[3] Low sulfur levels are desirable not only to appease EPA regulations but also to prevent fuel cell poisoning and catalyst deactivation.[4] Fuel cell vehicles are seeing a resurgence in interest for large-scale production and as a green solution to emissions from conventional vehicles.[5] However, the presence of sulfur in the fuel is a serious challenge that needs to be addressed before the systemic implementation of fuel cells.[6]

Recent reviews have discussed promising alternative approaches to HDS in great detail.[7,8] Among these alternatives, adsorptive desulfurization (ADS) has proven to be an effective method that can provide zero sulfur level fuels at ambient conditions.[9] Adsorbents are advantageous because they can be tailored to enhance the selectivity for sulfur compounds or increase the adsorption rates. Different types of sorbents may be used for ADS such as activated carbons,[10,11] metal–organic frameworks (MOFs),[12,13] metal oxides,[14,15] silica-based sorbents,[16,17] and zeolites.[18,19] Among them, faujasite (FAU) type zeolites are desirable for adsorption applications due to their unique pore structure and available active sites.

Zeolites are naturally occurring aluminosilicates that can be ion exchanged with cations; this property makes them appealing for a broad range of applications. A low Si/Al ratio zeolite indicates a higher capacity for ion exchange and is ideal for adsorption studies. Zeolite Y is a FAU zeolite with 7.4 Å sodalite cages and 12 Å supercages, which allow guest molecules access to the inner sites while preventing larger molecules from entering.[20] Consequently, Y zeolite is unable to adsorb molecules with a large kinetic diameter, such as refractory sulfur compounds (e.g., dibenzothiophene (DBT) and 4,6-dimethyldibenzothiophene (4,6-DMDBT)). The

Received: February 5, 2021
Revised: April 9, 2021
Published: April 22, 2021

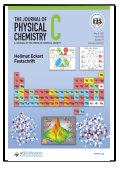

kinetic diameters of these compounds are at least 9 Å.[21] Our group has previously shown that introducing mesopores in the zeolite overcomes mass transport limitations to allow for successful adsorption of DBT.[22]

Y zeolite has Brønsted acid sites that can be ion exchanged with metal ions to enhance the selectivity for sulfur. Aromatics found in hydrocarbon fuels adsorb competitively with similarly sized sulfur compounds, decreasing the efficacy of the sorbent.[23] In order for a sorbent to be industrially viable, it must be selective in sulfur compounds over aromatic compounds. Yang et al. showed that Cu exchanged into zeolite Y may exhibit slightly higher selectivity toward thiophene compared to benzene, through weak σ-bonding, which is expected to be severely affected when the concentration of aromatics is high.[24] Velu et al. discovered that Ce exchanged Y zeolites are more selective toward sulfur compounds than aromatics due to strong direct sulfur−adsorbent interaction instead of π-complexation.[3] Shan et al. developed a bimetallic CuCeY zeolite that combines both adsorption modes, π-complexation and direct (S−M) σ bonds, resulting in improved adsorption performance of benzothiophene (BT) in the presence of aromatics.[25,26]

Tian and co-workers tested the adsorption performance of Ce exchanged mesoporous Y and found that mesoporosity decreased the mass transfer limitations and, as a result, improved the desulfurization performance of thiophene (TP) and BT.[27] Lee et al. tested Cu and Ce exchanged mesoporous zeolites for BT and DBT adsorption and found that Cu adsorbs via a π-complexation, whereas Ce adsorbs via both π-complexation and direct interaction with the metal (S−M).[28] From these promising results, they proceeded to show that mesoporous CuCeY is an effective sorbent for DBT and 4,6-DMDBT in the presence of aromatics.[22,29] The combination of Cu and Ce in Y zeolites has been well-documented as a promising sorbent, with both metals acting synergistically with each other. The question arises as to whether there is a measurable cause to this phenomenon and whether it can be observed with other bimetallic pairings.

This study focuses on understanding the role of rare earths (REs) such as Ce, La, Sm, and Nd as well as their synergistic behavior with Cu on the adsorption of BT and DBT in the presence of aromatics. Monometallic REs and bimetallic CuREs were exchanged in Y zeolites and were studied for the adsorption of BT. Analogous mesoporous Y materials, RESAY and CuRESAY, were studied for the adsorption of DBT. All samples were subjected to fixed-bed continuous adsorption experiments, and the results were used to calculate adsorption capacities. Spectroscopic studies were performed to determine the bonding mechanism and binding strengths of the REs. Rietveld refinement was performed to investigate the location and composition of metal cations in RE-modified zeolites. To the best of our knowledge, there has been no previous systematic study of the ADS of BT and DBT using various REY and bimetallic Cu-REY and their mesoporous counterparts.[30,31]

2. MATERIALS AND METHODS

2.1. Preparation of Metal Exchanged Zeolites. NH_4Y (Si/Al = 2.43) was purchased from Zeolyst International. Mesoporosity was introduced by using the surfactant-assisted (SA) method. Details surrounding the preparation of materials can be found elsewhere.[32,33] Information outlining the conditions and procedure has been described in our previous work.[28] For all mesoporous zeolites, mesoporosity was introduced prior to ion exchange and materials prepared through the SA method are labeled as "SAY". Cu and RE nitrates were used as a source for the cations. REY samples were ion exchanged to 5 wt % RE, and bimetallic samples were exchanged until 2.5 wt % Cu and 2.5 wt % RE have been reached. For the bimetallic samples, RE was exchanged first, followed by Cu, similar to our previous studies.[22,25] After ion exchange, samples were centrifuged, dried in air, and calcined at 525 °C for 5 h.

2.2. Model Fuel Preparation. Two model fuels were prepared: (a) 100 ppm BT in 20 wt % benzene and 80 wt % *n*-octane and (b) 100 ppm DBT with 1 wt % naphthalene in *n*-octane. Benzene and naphthalene were used to represent competing aromatic compounds that are commonly found in gasoline and diesel, respectively. The respective contents of aromatics and sulfur compounds were chosen to remain consistent with our previous studies[22,28] and to accurately represent commercial jet and diesel fuels.[34,35] All reagents used to prepare the model fuels were purchased from Sigma-Aldrich.

2.3. Material Characterization. The materials were subjected to characterization using a variety of techniques. The crystalline structure was determined by X-ray diffractometer (XRD) using a Bruker D2 phaser diffractometer. N_2 adsorption−desorption studies using a Micromeritics ASAP2020 were used to determine surface properties and analyzed by using the Brunaeur, Emmert, and Teller (BET) method. Metal loadings on the zeolite were quantified by using inductively coupled plasma optic emission spectroscopy (ICP-EOS) and X-ray fluorescence (XRF). Pyridine adsorption studies and temperature-programmed desorption (TPD) of TP were performed by using a Nicolet 6700 Fourier transform infrared spectrometer (FTIR) equipped with a diffuse reflectance (DRIFT) cell by Harrick. Temperature-programmed reduction (TPR) studies were performed by using 10% H_2 gas from 50 to 650 °C at a ramp rate of 10 °C/min.

2.4. Liquid Adsorption Studies. Dynamic fixed bed desulfurization studies were conducted by using a custom system consisting of 1/4 in. quartz tubing 26 cm long that was packed with sorbent. Between 0.2 and 0.3 g of sample was loaded into the column to reach a consistent bed height of 3 cm. Metal-containing catalysts were activated by flowing H_2 gas at 450 °C for 2 h and cooled to room temperature while maintaining H_2 flow. According to the H_2-TPR studies presented in Figure S4, such conditions are sufficient to maintain Cu in the monovalent state. The two reduction peaks at 250 and 350 °C shown in Figure S4a for CuY correspond to the reduction of Cu^{2+} to Cu^{+} in the supercage and sodalite cage, respectively. A much higher temperature (over 700 °C) is required to further reduce Cu^{+} to Cu^{0} according to the literature.[36] TPR profiles of other RE and CuREY zeolites are also provided in this figure for reference. When the system reached ambient conditions, the H_2 flow was stopped and model fuel was pumped into the top of the column at 0.05 mL/min. Gas chromatograph (GC) sample vials were placed at the exit of the column to collect 0.5 mL of effluent at regular intervals. Collected samples were analyzed by an Agilent 7890A gas chromatograph equipped with an Agilent 355 sulfur chemiluminescence detector (SCD).

2.5. TPD Studies Using DRIFTS. The DRIFTS system was used to determine the adsorptive mechanism and bonding type through sulfur TPD experiments. The FTIR was connected to a stainless-steel line, mass flow controllers, and

https://doi.org/10.1021/acs.jpcc.1c01103
J. Phys. Chem. C 2021, 125, 9107−9118

an Edwards T-Station 75 turbomolecular vacuum pump, which allows the *in situ* study of sulfur adsorption and desorption. Each spectrum was taken by using 32 scans with a resolution of 4 cm^{-1} in increments of 50 °C from 50 to 350 °C. Between 20 and 30 mg of zeolite powder was placed in the sample holder before degassing at 450 °C. The sample was then cooled to 50 °C, at which BT vapor was allowed to flow into the cell. After reaching saturation, the sample was purged, evacuated, and desorbed until the original sample was regenerated. All spectra were analyzed by using the OMNIC 9.4 software.

2.6. Rietveld Refinement. XRD data for Rietveld refinement were acquired with a Bruker D2 Phaser diffractometer equipped with a high-speed linear detector (LYNXEYE) and Cu Kα radiation (λ = 1.54184 Å) at 30 kV and 10 mA. The measurements were performed at room temperature over 2θ = 5°−95° with a scan speed of 1 s/step and a step size of 0.02°. However, only powder data ranging from 15° to 60° were processed to avoid peak asymmetry. The Rietveld analysis was performed with the software package GSAS-II (General Structure Analysis System) by using the Rietveld method.[37] The space group of NH_4Y is $Fd\bar{3}m$ as it exhibits a FAU framework with lattice parameter $a \approx 24.6$ Å. The crystallography information about the Y zeolite was taken from the International Zeolite Association (IZA) database.[38] For the initial structure model, the framework coordinates of REY were adopted from Du et al.[39] The initial values of the occupancy factor were obtained from XRF and ICP-OES results. Al and Si were treated as similar atoms as they occupy the same general position by imposing constraints on their thermal parameter (u_{iso}), fractional occupancy (frac) and positions (x, y, and z). Subsequently, bond distances of Si−O and Al−O were restrained to 1.59 and 1.71 Å, respectively. To determine the best possible fit to the data, the LeBail extraction method was first conducted.[40] Background was fit by using a Chebyschev polynomial function with 8 number of coefficients. The refinement was performed by first optimizing the unit cell and scale factor. Subsequently, difference Fourier maps were generated to locate unaccounted electron density due to missing atoms. Missing atom locations were filled with either an oxygen atom to account for any physisorbed water, RE atoms, or Cu atoms for the bimetallic cases. The updated structure with the newly added atoms was refined until low weighted residual error (R_{wp}) and goodness of fit (GOF) were achieved.

3. RESULTS

3.1. Characterization of Materials. N_2 adsorption−desorption experiments were performed to measure the surface area and the micropore and mesopore volume of all the zeolites. As expected, the surface area and the micropore volume slight decreased when metals were introduced in the structure. The introduction of mesoporosity in the Y zeolite is evident by the significant increase in mesopore volume in the SAY sample from 0.051 to 0.172 m^2/g. More details regarding the mesoporous zeolite and their characteristics can be found in our previous studies.[22,28] ICP-OES was used to quantify the metal loading of all zeolites. The RE target loading for REY was 5 wt %, and the RE and Cu target loadings for the bimetallic CuREY were 2.5 and 2.5 wt %, respectively. This target was achieved for all of the samples within a small degree of error. The physicochemical properties of the all the zeolites can be found in Table 1. All of the zeolites were also subjected to XRD analysis. The patterns of Y and REY zeolites can be found in Figure 1. A slight decrease in intensity of the peaks of the RE exchanged zeolites relative to the parent zeolite was observed, but the characteristic peaks observed in parent Y were mostly preserved. No oxide peaks for RE exchanged materials and no shifts were observed. These findings suggest that the ion exchange and calcination steps did not impose significant damage on the structure of the zeolite, and very little to no oxides were formed. In our previous studies we have also shown that the introduction of mesoporosity imposes a slight decrease in intensity of the XRD peaks relative to the Y, which suggests some destruction of the crystalline structure.[22,28]

Table 1. Surface Area, Micropore as Well as Mesopore Volume, and Metal Contents of All Zeolites Tested

samples	S_{tot} (m^2/g)	V_{tot} (cm^3/g)	V_{micro} (cm^3/g)	V_{meso} (cm^3/g)	RE (wt %)[a]	Cu (wt %)[a]
parent Y	640	0.323	0.272	0.051		
LaY	628	0.305	0.262	0.043	4.9	
NdY	604	0.303	0.255	0.048	5.0	
SmY	626	0.316	0.265	0.051	4.7	
CeY	610	0.309	0.259	0.05	5.1	
CuLaY	653	0.329	0.28	0.049	2.3	2.5
CuNdY	627	0.327	0.271	0.056	2.6	2.8
CuSmY	632	0.32	0.271	0.049	2.4	2.5
CuCeY	624	0.32	0.267	0.053	2.5	2.2
SAY	641	0.367	0.195	0.172		
LaSAY	609	0.362	0.184	0.178	3.5	
NdSAY	709	0.409	0.166	0.243	3.8	
SmSAY	632	0.364	0.147	0.217	4.6	
CeSAY	656	0.378	0.156	0.222	4.3	
CuLaSAY	620	0.377	0.184	0.193	2.3	2.6
CuNdSAY	633	0.319	0.159	0.16	2.1	1.9
CuSmSAY	652	0.352	0.173	0.179	2.0	2.2
CuCeSAY	640	0.361	0.149	0.212	2.4	2.1

[a]ICP-OES measurements.

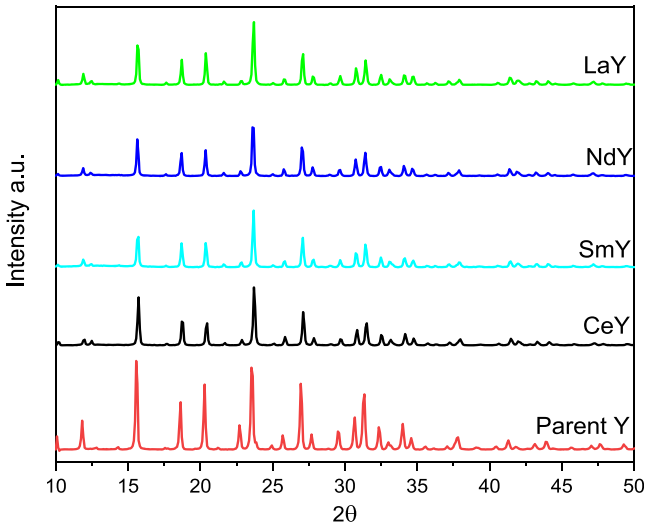

Figure 1. X-ray diffraction patterns of parent and rare earth exchanged zeolite Y.

Brønsted acid sites (BAS) and Lewis acid sites (LAS) were quantified by using pyridine FTIR. Pyridine is commonly used for acidity quantification due to its ability to form pyridium with BAS and bond with LAS via electron transfer, both of

https://doi.org/10.1021/acs.jpcc.1c01103
J. Phys. Chem. C 2021, 125, 9107−9118

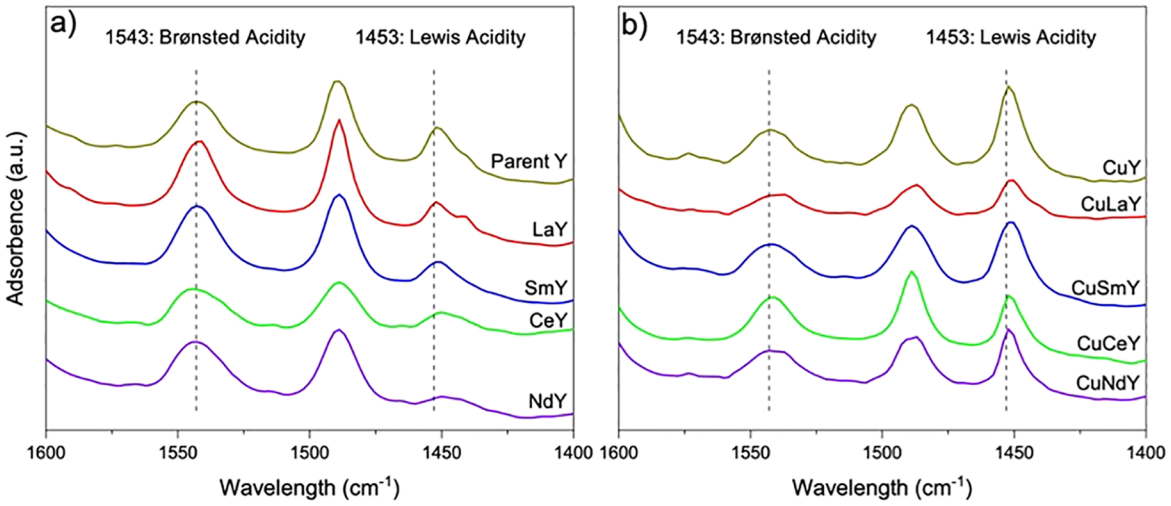

Figure 2. FTIR pyridine results of (a) parent Y, CuY, and REY and (b) bimetallic CuREY zeolites.

which can be detected by FTIR. Figure 2 shows the spectra associated with the pyridine adsorption studies for both single-metal REY and bimetallic CuREY zeolites. The peak at 1543 cm^{-1} corresponds to the BAS, while the peak at 1453 cm^{-1} corresponds to LAS. The peaks can be integrated to quantify the amount of acid sites normalized by sample weight, and the results can be found in Table 2. The parent Y had a large amount of BAS which is expected due to the amount of framework alumina. Acidity decreased after the exchange of REs, which agrees with previous studies using La and Ce.[41,42] This can be attributed to the replacement of the hydrogen of the Brønsted acid sites with REs during ion exchange, decreasing the amount of available sites detectable by using pyridine. The effect of introduction of mesoporosity in the Y zeolite has been discussed in our previous work where we showed a slight decrease in BAS.[28] The introduction of Cu in the bimetallic CuREY zeolites further reduces the Brønsted acidity and increases the Lewis acidity of the REY zeolites, which results in a low Brønsted to Lewis ratio of the CuREY zeolites. According to the Lewis acid−base theory, Lewis acidity plays a significant role in sulfur adsorption by adsorbing acid bases, such as thiophenes, more easily.[43]

Table 2. FTIR Pyridine Results of Parent Y, CuY, REY, and CuREY Exchanged Zeolites

zeolite sample	Brønsted acidity (μmol/g cat.)	Lewis acidity (μmol/g cat.)	ratio (B/L)
parent Y	51.1	33.1	1.54
CuY	25.8	47.7	0.54
LaY	41.9	16.5	2.54
CuLaY	14.3	21.2	0.67
SmY	44.2	14.5	2.90
CuSmY	36.0	45.2	0.80
CeY	35.4	11.3	3.13
CuCeY	31.5	30.5	1.03
NdY	55.2	11.7	4.70
CuNdY	29.6	35.0	0.85

3.2. Adsorption Results. *3.2.1. Benzothiophene Adsorption.* Liquid ADS experiments were conducted by using BT in a mixture of 20 wt % benzene and 80 wt % octane on RE and CuRE exchanged Y. The resulting breakthrough curves can be found in Figure 3. The parent Y zeolite produced effluent containing sulfur upon exposure to the model fuel, indicating a low adsorption of sulfur. When REs were exchanged in Y, the breakthrough curves shifted to the right, indicating an increase

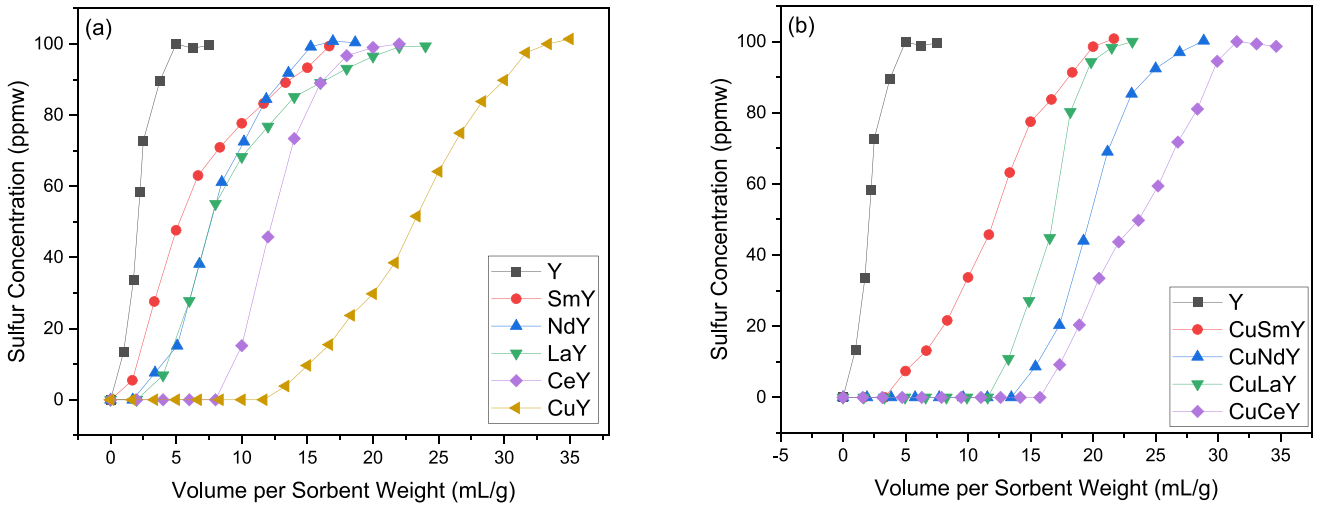

Figure 3. Breakthrough curves of 100 ppm BT in octane with 20 wt % benzene on (a) RE and Cu exchanged Y and (b) CuRE exchanged Y.

https://doi.org/10.1021/acs.jpcc.1c01103
J. Phys. Chem. C 2021, 125, 9107−9118

in the adsorption capacity. SmY increased the breakthrough point of HY by only 2 mL/g. NdY and LaY had a similar but later breakthrough point compared to SmY. CeY had the most extended breakthrough point of 7.5 mL/g, indicating that it had the highest sulfur capacity out of all the REY tested.

As stated previously, Cu has proven to be effective at adsorbing sulfur compounds when ion exchanged with zeolite Y. When Cu is added to CeY, the adsorption performance is known to behave better than Cu and Ce independently.[25,28] Breakthrough curves containing bimetallic Cu-REY can be found in Figure 3b. An immediate increase in capacity can be observed when compared to Figure 3a. The addition of Cu doubled the breakthrough point of SmY and nearly tripled the breakthrough point of the other REs tested. CuCeY was found to have the highest capacity out of all the bimetallic combinations tested. The effect of Cu on the adsorption capacity of REY zeolites can be more clearly seen in Figure 4.

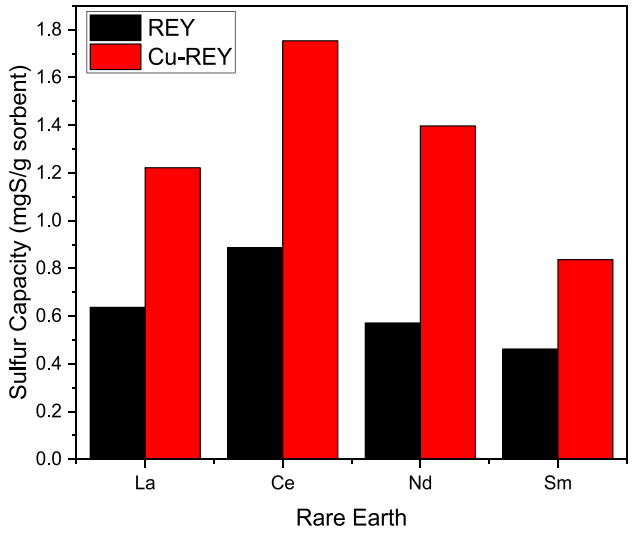

Figure 4. Comparison between sulfur capacities of REY and CuREY from fixed bed adsorption experiments using 100 ppm BT in octane containing 20 wt % benzene.

The capacity was derived from the breakthrough curves, and details on the calculations are given in the Supporting Information. Figure 4 shows the promoting effect of Cu on the adsorption capacity of all the sorbents, with CuCeY displaying the highest adsorption capacity of ~1.7 mg of S/g.

3.2.2. Dibenzothiophene Adsorption. While BT is mainly found in gasoline range fuels, DBT is the dominant sulfur molecule in diesel fuels. To better represent a model diesel fuel, naphthalene was used as the aromatic compound that would adsorb competitively with DBT. Figure 5 shows the breakthrough curves of DBT in octane containing 1 wt % naphthalene using mesoporous zeolites. The induced mesoporosity increased the sulfur capacity of all of the zeolites due to the decrease in mass transfer limitations, which we have demonstrated previously.[22]

SmSAY did not increase the adsorption of DBT compared to the parent SAY, suggesting that Sm is not active toward DBT. Conversely, the addition of Nd, La, and Ce cations improved the performance of the parent SAY. When Cu was added in addition to the RE for CuRESAYs, an immediate difference was observed. The DBT capacities for each RE species are greater in the CuRESAY material than in RESAY. Figure 5a shows that Sm did not increase the capacity of DBT compared to the parent Y zeolite, so it can be assumed that all of the adsorption in the bimetallic sorbents in Figure 5b can be attributed to Cu. CuNdSAY adsorbed sulfur until 20 mL/g and reached saturation relatively quickly. CuLaSAY produced zero sulfur level fuel for nearly double the volume, around 40 mL/g. CuCeSAY was the best performing sorbent in this study, with a breakthrough point around 45 mL/g.

Similar to Figure 4, Figure 6 shows the adsorption capacities derived from the breakthrough curves of RESAY and Cu-RESAY samples for DBT adsorption in the presence of naphthalene. The sorbents showed similar trend for DBT and BT adsorption capacities. One deviation from BT adsorption is the performance of La, which is close to that of Ce. Another observation was that the addition of Cu in the RE sorbents increased the capacity for DBT to a greater extent than for BT, suggesting a stronger adsorption on larger thiophenic compounds, as indicated elsewhere.[22]

3.3. *In Situ* DRIFTS Studies. The mechanism of adsorption of sulfur compounds in zeolites depends on the

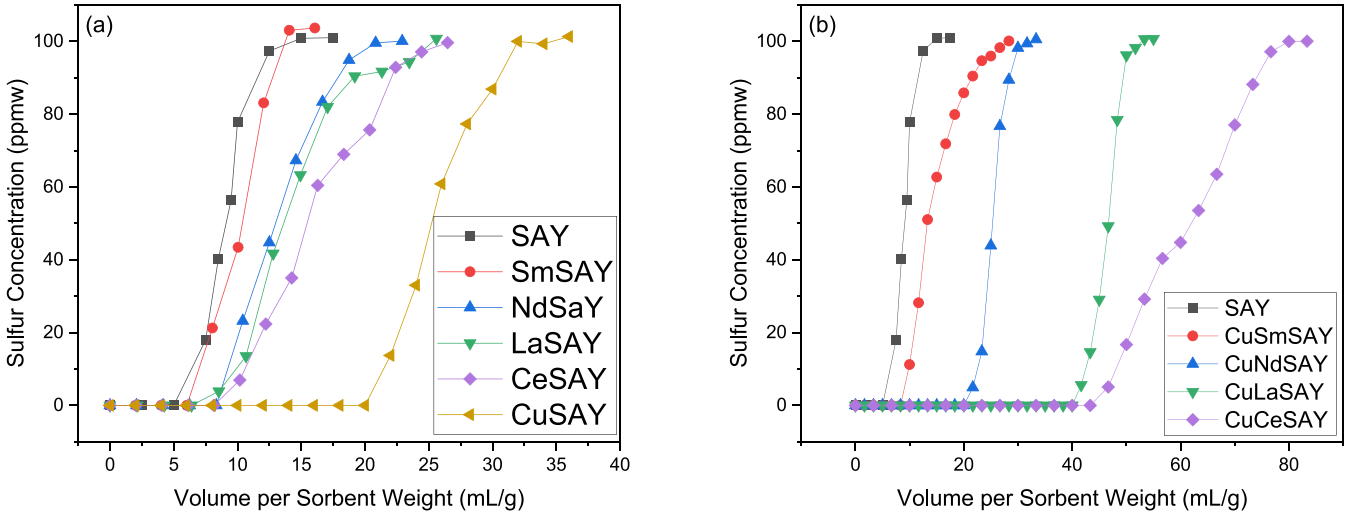

Figure 5. Breakthrough curves of 100 ppm DBT in octane with 1 wt % naphthalene on (a) RESAY and (b) CuRESAY.

https://doi.org/10.1021/acs.jpcc.1c01103
J. Phys. Chem. C 2021, 125, 9107−9118

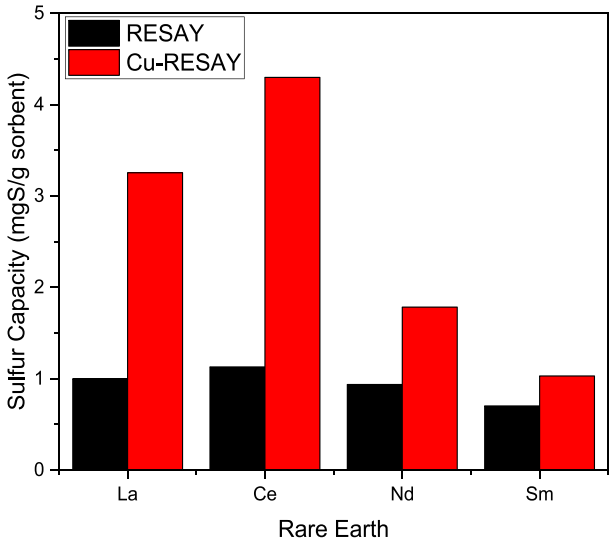

Figure 6. Comparison between sulfur capacities of mesoporous bimetallic zeolites found through fixed bed adsorption experiment using 100 ppm DBT in octane containing 1 wt % naphthalene.

metals in the zeolite and the zeolite−metal interactions.[24,44] *In situ* DRIFTS experiments were conducted by using BT as the model compound to understand the mechanism of sulfur adsorption on REs zeolites. Figure 7a shows the FTIR spectra of REY after exposure to BT vapor, highlighting coordination between BT and the RE metals. The spectra show the peaks between 1800 and 1400 cm^{-1} as they are mostly responsible for the C═C double bond in the aromatic ring of BT.

As BT flows over the samples, no immediate changes can be seen in the wavenumber range shown in Figure 7a. Some physisorbed moisture may be present in the DRIFTS cell, which increases the baseline of the spectrum and consequently prevents the detection of chemisorption peaks due to sulfur after exposure to BT. After evacuation, several characteristic peaks arise at 1630, 1585, 1490, 1455, and 1425 cm^{-1}. The peak at 1630 cm^{-1} can be attributed to adsorbed moisture and disappears as the sample is heated leading to desorption of water molecules. The two peaks at 1585 and 1455 cm^{-1} are typical characteristics of sulfur adsorption on Y zeolites.[22] The other peaks can be explained by looking at the spectrum of free BT in Figure S1, showing the symmetrical C═C vibrational mode at 1460 cm^{-1}. Upon adsorption of BT, this aforementioned 1460 cm^{-1} peak can undergo either a blue-shift or a red-shift depending on the mechanism of adsorption. In Figure 7a, the 1460 cm^{-1} peak can be seen to undergo a blue-shift of 30 cm^{-1} to 1490 cm^{-1}. This blue-shift represents an increased electron density within the C═C−C═C fragment of BT, indicating that the S atom is interacting directly with the RE ion through (S−M) σ bonding.[45] Conversely, the peak at 1425 cm^{-1} can be interpreted as a red-shift of the characteristic symmetrical vibrational mode at 1460 cm^{-1} for free BT. A reduction in wavenumber can be correlated to a decrease in electron density of the adsorbing species. This suggests that the aromatic ring of BT was adsorbed parallel to the surface, indicating the presence of π interactions.[46] Both characteristic modes, direct S−M and π complexation, are found in all the REY samples, suggesting that the mechanism of adsorption is the same between the samples. To understand the effect of the addition of Cu, we performed *in situ* DRIFTS tests for all the CuREY zeolites. The spectra are shown in Figure 7b. It appears that after evacuation of benzothiophene all the bimetallic CuREY zeolites show the characteristic peaks of π complexation and σ bonding at 1490 and 1425 cm^{-1}, respectively. However, in all CuRE samples the band at 1425 cm^{-1} is more intense compared to their corresponding REY zeolite. This suggests that the presence of Cu increases the capacity for sulfur adsorption via π-complexation, which could contribute to the increased adsorption capacity observed in CuREY zeolites compared to their REY counterparts. Nonetheless, a reduction in peak intensity at 1425 cm^{-1} can be seen at 300 °C, indicating the breaking of some sulfur π complexes.

3.4. Rietveld Refinement. The structural parameters and metal composition of all the RE and CuRE exchanged Y zeolites were further studied by using Rietveld refinement. The corresponding CeY and CuCeY refinement results are shown in Table 3, and the observed, calculated, and differential XRD patterns are shown in Figure 8. The refinement results of all the other zeolites, including LaY, SmY, and NdY, and bimetallic zeolites CuLaY, CuSmY, and CuNdY as well as their experimental and calculated XRD patterns are presented in Table S1 and Figure S2, respectively. All zeolites were similarly refined, and the calculated residual errors, GOF, unit cell size, and number of cations in coordination sites as obtained by the refinement and XRF measurements are presented in Table 4. The main crystal structures of the exchanged zeolites did not differ evidently.

Figure 8a and Table 4 show that the Rietveld refinement of CeY has converged with low R_{wp} and GOF values, giving a unit cell size of 24.55 Å. The structure refinement result of CeY indicates that there are Ce cations on sites I′ (SI′) and II′ (SII′), with a total of 7.38 Ce atoms in the sodalite cages. This occupancy number is close to the Ce concentration calculated by XRF, as shown in Table 4. The location of Ce in SI′ and SII′ indicates that the ion exchanged Ce cations have migrated from the supercages to the internal cages upon calcination. Our previous study using X-ray photoelectron spectroscopy (XPS) showed that Ce located on the surface are mostly in the 4+ oxidation state.[29] Other studies have demonstrated that Ce cations in the sodalite cage are mostly in the 3+ oxidation state to form highly stabilized coordination with nearby framework oxygens.[47] Thus, we hypothesize that most of the Ce in the sodalite cages should be in the 3+ oxidation state. However, more experiments are needed to confirm this hypothesis. Table 3 shows that while Ce cations tend to populate coordination sites inside the sodalite cage, the presence of water is inevitable at site II (SII), as Y zeolites are prone to adsorbing water moisture from air. A visual representation of the Y zeolite and the corresponding coordination sites can be found in Figure S3. To better understand the location of the cations within the zeolite, the interatomic distances between the cations and the framework oxygens are shown in Table S2. In SI′, the 0.36 Å greater bond length of Ce(I′)−O2 compared to Ce(I′)−O3 suggests a stronger coordination between Ce and O3 due to electrostatic repulsion between nearby Ce cations.[48,49] Conversely, in SII′, Ce(II′)−O3 exhibits a longer bond length compared with Ce(II′)−O2.

Rietveld refinement results of other RE exchanged Y zeolites can be found in Tables S2 and S3 as well as Figure S2. To validate our model, the average T−O distance was calculated to be ∼1.65 Å, which is in good agreement with previous literature[50] as well as the crystallography data from IZA.[38] Figure 8b and Table 3 display the Rietveld analysis of the

https://doi.org/10.1021/acs.jpcc.1c01103
J. Phys. Chem. C 2021, 125, 9107−9118

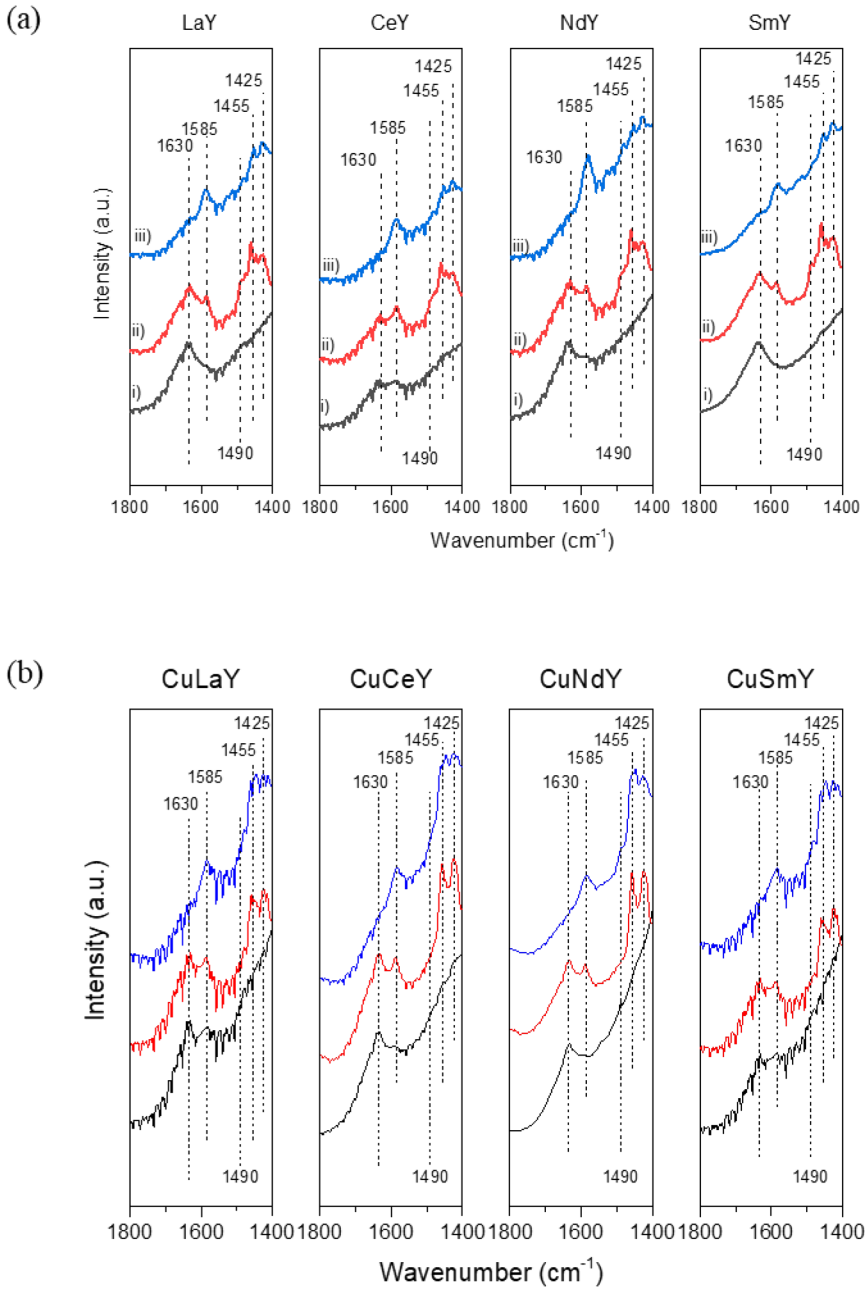

Figure 7. *In situ* DRIFTS spectra of (a) REY and (b) CuREY zeolites after (i) exposure to BT vapor, (ii) evacuation at 50 °C, and (iii) 300 °C under vacuum.

CuCeY zeolite. The slightly increased R_{wp} and GOF values compared to CeY can be attributed to the difference in diffraction peaks at lower angle. This suggests the greater complexity of the bimetallic system. Nonetheless, the fractional occupancies of cations are in relatively close agreement with the chemical composition obtained from XRF analysis in Table 4. The experimental and calculated XRD patterns of other bimetallic CuREY zeolites are shown in Figure S2. Table 4 shows that in CuCeY Ce cations occupy SI′ and SII′, and Cu cations occupy SII. The total Ce and Cu occupancies reported from the refinement are in close agreement with XRF data, with Cu in SII showing much greater site occupancy than the Ce sites SI′ and SII′. Cu close to the supercage in SII are predominantly Cu^{2+} as a result of rapid oxidation of Cu^{+} in air.[29] As opposed to CeY, the introduction of Cu in CuCeY displaces the water molecules from SII, which may explain the increase in adsorption capacity in our adsorption experiments. Table S2 also shows the bond distances of bimetallic cations and nearby framework oxygen atoms. Similar to CeY, Ce(I′)−O3 and Ce(II′)−O3 exhibit shorter and longer bond lengths, respectively, than Ce(I′)−O2 and Ce(II′)−O2, confirming the strong coordination or repulsion of cations within the respective framework oxygens. Because Cu cations in CuCeY are located inside the supercage, sulfur compounds might be able to access these adsorption sites more easily and form relatively strong π-complexation. This might be the reason an increase in capacity is shown by CuCeY in the fixed-bed adsorption experiments. The presence of water molecules in the supercage inhibits the adsorption of sulfur on the internal

https://doi.org/10.1021/acs.jpcc.1c01103
J. Phys. Chem. C 2021, 125, 9107−9118

Table 3. Final Structure Model of CeY and CuCeY Based on Rietveld Refinement

atom	x	y	z	frac	multi	no. of atoms/uc
CeY						
Si	−0.0527	0.1277	0.0355	0.7212	192	138.5
Al	−0.0527	0.1277	0.0355	0.2788	192	53.5
O1	0.0000	−0.1062	−0.1062	1.0000	96	96.0
O2	0.0003	0.0003	0.1397	1.0000	96	96.0
O3	0.0757	0.0757	−0.0347	1.0000	96	96.0
O4	0.0707	0.0707	0.3256	1.0000	96	96.0
Na(I)	0.0000	0.0000	0.0000	0.5249	16	8.4
Ce(I′)	0.0745	0.0745	0.0745	0.1658	32	5.3
Ce(II′)	0.1508	0.1508	0.1508	0.0650	32	2.1
OW(II)	0.2868	0.2868	0.2868	0.5717	32	18.3
CuCeY						
Si	−0.0541	0.1273	0.0369	0.7212	192	138.5
Al	−0.0541	0.1273	0.0369	0.2788	192	53.5
O1	0.0000	−0.1033	0.1033	1.0000	96	96.0
O2	−0.0014	−0.0014	−0.0014	1.0000	96	96.0
O3	0.0730	0.0730	−0.0379	1.0000	96	96.0
O4	0.0706	0.0706	0.3238	1.0000	96	96.0
Na(I)	0.0000	0.0000	0.0000	0.5664	16	9.1
Ce(I′)	0.0690	0. 0690	0. 0690	0.0685	32	2.2
Ce(II′)	0.1459	0. 1459	0. 1459	0.0325	32	1.0
Cu(II)	0.3002	0. 3002	0. 3002	0.2244	32	7.2

active sites, thereby reducing the capacity of single-metal REY zeolites.

The refinement results in Table S2 show that almost all the RE cations are located on SI′ and SII′, suggesting that the RE cations had been well dispersed or had entered the structure of Y zeolite. Subsequently, either water or Cu cations can occupy SII. Table 4 presents the R_{wp} and GOF values of Rietveld refinement on all zeolite samples. The low values of R_{wp} suggest reliability of the results. Table 4 also shows additional information regarding the cation population on SI′, SII′, and SII of all the studied zeolites, comparing values obtained by Rietveld refinement and XRF elemental analysis. The resulting unit cell compositions of all REY and CuREY are also presented in Table S3. The number of atoms per site was determined by using the fractional occupancy and site multiplicity generated from the refinement. RE atoms were found on SI′ and SII′ for all of the samples. In bimetallic zeolites, Cu is located in SII, which is in agreement with previous experimental studies.[51,52] The unit cell size is similar for all the zeolites, having been reduced from the parent HY (24.68 Å) due to some loss in framework alumina during the ion exchange. Nonetheless, it has been suggested that the reduced unit cell parameters are not related to the corresponding ion exchanged metals or bond lengths.[39] As stated previously, the metal composition from Rietveld refinement is consistent with those from ICP and XRF elemental analyses validating the integrity of these methods when used in tandem of each other.

4. DISCUSSION

The current desulfurization process of HDS has challenges in removing large refractory sulfur compounds without the requirement of stringent conditions, calling for alternative more efficient methods. This study investigates the method of ADS using RE exchanged Y zeolite as a promising complementary method to HDS. Work was previously conducted on the nature of CeY and LaY, but only a few studies have been performed on SmY and NdY as well as bimetallic combinations of the aforementioned rare REs with other metals.[30,31,53] The work presented in this paper shows characterization and ADS results for CeY, LaY, SmY, NdY, and the corresponding CuREY zeolites as well as their mesoporous counterparts.

Figure 3 shows the breakthrough curves of BT in *n*-octane for REY and CuREY in the presence of benzene. The introduction of the REs increases the adsorption performance of the parent Y zeolite. Overall, the adsorption performance of REY for BT is comparable for all REs, with CeY standing out as the best with breakthrough point of 10 mL/g and sulfur capacity of 0.84 mg of S/g. Figure 4 shows that the addition of Cu in the REY zeolites improves their performance. CeCuY performed the best out of all the bimetallic zeolites with breakthrough point of 16 mL/g and total sulfur capacity of 1.76 mgS/g in the presence of benzene. Mesoporous SAY materials were not tested for BT adsorption because BT is small enough to access the inner active sites of the Y zeolite.[28]

Mesoporosity was successfully introduced into zeolite Y and confirmed by porosity measurements. Figure 5a shows the adsorption of DBT on RESAY. A better adsorption performance can be observed compared to the parent SAY. However, all the RESAY had a similar breakthrough point, and CeSAY had the largest sulfur capacity of 1.1 mg of S/g. The addition of Cu greatly increased the adsorption performance of all the RESAY samples tested. The trend is the same as in the case of BT adsorption with CuCeSAY performing the best out of all the bimetallic zeolites. The breakthrough point of CuCeSAY was 44 mL/g, almost 4 times higher than the breakthrough point of CeSAY, suggesting a strong synergistic effect between Cu and Ce.

FTIR studies were performed to obtain information about the mechanism behind sulfur adsorption on RE atoms. Pyridine IR experiments showed that when Cu is introduced in the REY zeolites, the Lewis acidity of the latter is significantly increased. According to the Lewis acid−base

https://doi.org/10.1021/acs.jpcc.1c01103
J. Phys. Chem. C 2021, 125, 9107−9118

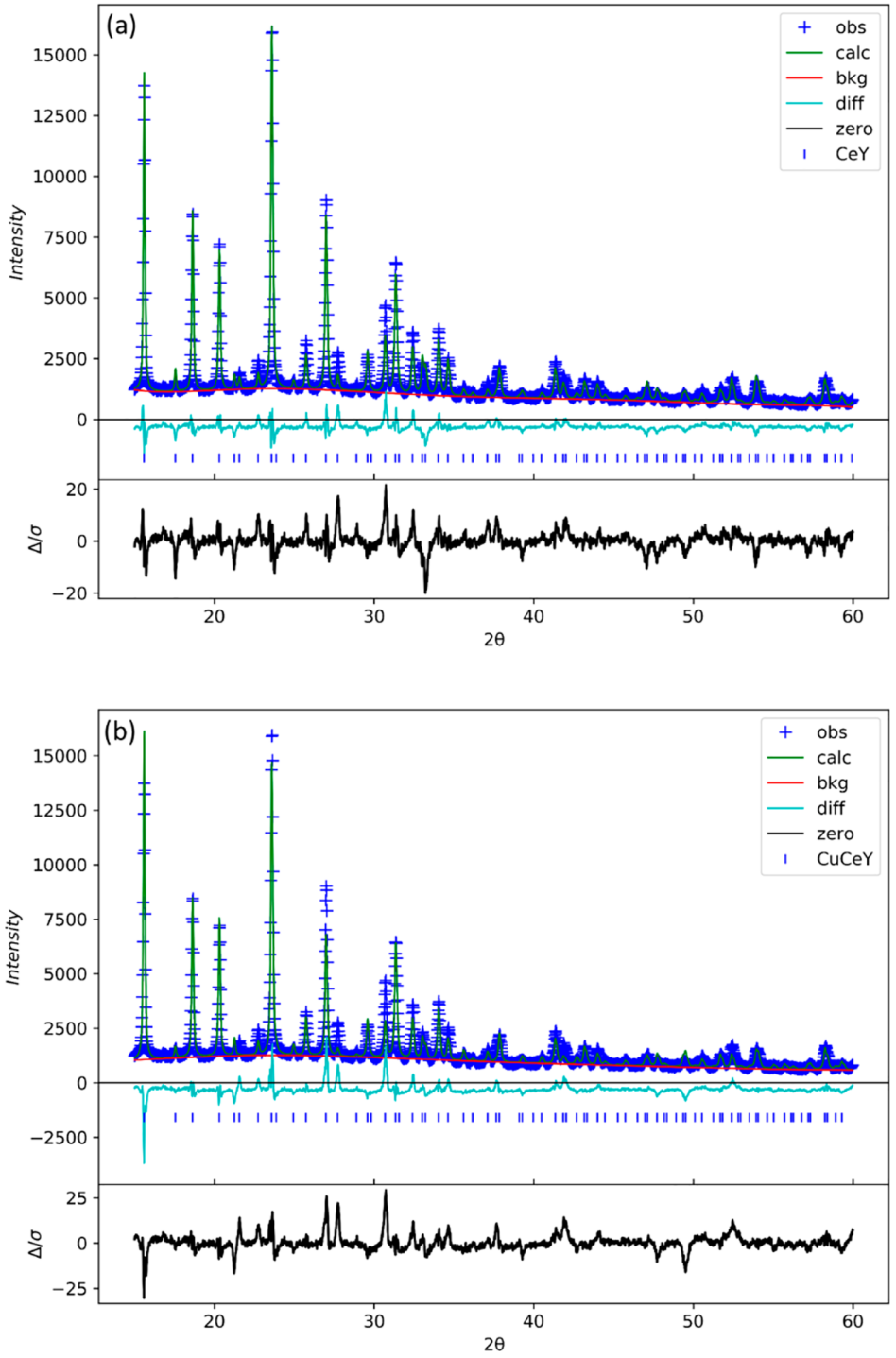

Figure 8. XRD pattern of the (a) CeY and (b) CuCeY refined by the Rietveld method. The ticks (+) correspond to experimental data, the green line corresponds to the calculated data, vertical bars (|) indicate the positions of Bragg peaks, and the bottom trace depicts the difference between the experimental and the calculated values.

theory, Lewis acidity can significantly enhance the sulfur adsorption by adsorbing acid bases, such as thiophenes.[43] This might be a possible explanation for the better adsorption performance of the CuREY zeolites. *In situ* DRIFTS studies have been performed by using benzothiophene as a probe molecule to identify the sulfur adsorption mechanism. The spectra can be found in Figure 7. All of the REYs displayed peaks at 1490 and 1425 cm^{-1}, suggesting direct σ bonding between metal ions and sulfur atoms and π complexation, respectively. When Cu was introduced in the REY zeolites the peak at 1425 cm^{-1} became more intense, suggesting a more enhanced π complexation, possibly due to the Cu. However, as the samples were heated, the peak responsible for π interaction decreased, indicating that σ bonding due to the RE might be more stable. Previous studies have found similar results for CeY, which exhibits relatively strong σ bonding interaction with sulfur which can only be broken at very high temperatures.[22,54] Furthermore, H_2-TPR studies have been performed to understand the oxidation state of metals in the REY and the CuREY zeolites (Figure S4). The TPR profile of

https://doi.org/10.1021/acs.jpcc.1c01103
J. Phys. Chem. C 2021, 125, 9107−9118

Table 4. Final Refinement Residual Errors, GOF, Unit Cell Size, and Number of Cations on All Coordination Sites

zeolites	R_{wp}	GOF	UCS[a] (Å)	RE(I′)[b]	RE(II′)[b]	Cu(II)[b]	RE[c]	Cu[c]
LaY	0.1074	3.25	24.573	4.71	2.38		6.98	
CuLaY	0.1006	3.51	24.659	2.36	0.60	7.38	3.48	7.18
CeY	0.0941	3.51	24.655	5.30	2.08		7.03	
CuCeY	0.1173	4.37	24.645	2.19	1.04	7.18	3.18	7.09
NdY	0.8090	2.62	24.652	2.35	1.82		7.02	
CuNdY	0.9169	3.29	24.666	2.63	0.64	7.26	3.37	7.88
SmY	0.0784	2.79	24.636	5.00	1.06		6.04	
CuSmY	0.0840	3.13	24.652	2.57	0.47	6.44	2.88	6.62

[a]Unit cell size. [b]Number of atoms obtained by using Rietveld refinement. [c]Number of atoms obtained by using XRF.

CuY showed two peaks for the reduction of Cu^{2+} ions to Cu^{+}; the lower temperature peak was associated the ions in the supercage, while the higher temperature peak was associated with the ions in the sodalite cage. This is in agreement with literature.[36] It also appeared that this reduction temperature was further reduced in the presence of REs. The easier reduction of Cu^{2+} ions in the presence of RE might also contribute to the improved sulfur adsorption of CuREY compared to the REY, since previous studies have demonstrated that Cu^{+} has higher sulfur adsorption capacity compared to Cu^{2+}.[55] However, more experimental evidence on the oxidation states of RE and CuREY zeolites is needed to better understand the bimetal zeolites.

Rietveld refinement was used to determine the locations and the amount of RE cations within the zeolite Y. Du et al. found that calcined LaY contains La cations populated in SI′ and SII, whereas noncalcined LaY only contained cations in SII.[48] One possible cause for the differences arising in performance between the REs might be the oxidation state of the cations. La, Sm, Nd, and Ce all have 3+ oxidation states, but Ce can also be present as Ce^{4+}. A larger valence implies that Ce has more electrons involved in bonding, and the ground electronic configuration is relatively strong.[56] Our previous work on Ce exchanged zeolite Y shows that Ce preferentially exists in the 4+ over the 3+ state when by itself and when paired with Cu.[29] However, other studies have demonstrated that when in the sodalite cage Ce prefers the 3+ state.[47] More research needs to be conducted to understand the role of the oxidation state on the adsorption performance of Ce. Another explanation for the remarkable adsorption capability of CuCeY can be attributed to the location and concentration of Cu in the supercage. Rietveld refinement has shown that the tendency of RE cations to migrate to SI′ and SII′ upon calcination allows Cu cations to occupy SII, the first adsorption sites that adsorbates interact within the supercage. Furthermore, Cu^{2+} cations close to the supercage are more easily reduced to Cu^{+}, which is highly desirable for sulfur adsorption. This is evident from our H_2-TPR studies shown in Figure S4. The TPR profile of CuY shows two peaks with the lower temperature peak associated with the reduction of Cu^{2+} ion located close to the supercage to Cu^{+}. The reduction temperature and peak intensity are further lowered with the addition of some REs. The ease of reduction of Cu ions may contribute to the improved sulfur adsorption of CuREYs. Previous studies have shown that Cu^{+} cations have the tendency to adsorb sulfur molecules via π complexation, which significantly enhances the desulfurization performance.[57] Our findings from Rietveld refinement are in good agreement with our experimental results. CuSmY reports the lowest Cu^{+} concentration in the supercage, validating the lowest adsorption capacity in our adsorption experiment. The fractional occupancies of La, Nd, and Ce are similar to each other. From the bond distances in Table S3 the Cu−O bonds in CuCeY are shorter compared to the other CuREY zeolites, indicating that the synergistic interaction between Cu and Ce is relatively strong, thereby improving the sulfur adsorption. Table 4 indicates that the Ce density (1.04) in CuCeY is the highest compared to other REs in bimetallic Y on SII′. This may lead to higher possibility of σ-bond interactions with sulfur. Nonetheless, there is an optimum point that must be reached between the concentration and the location of Cu^{+} and RE metals to achieve the greatest sulfur adsorption capacity.

5. CONCLUSION

This work explored the potential of REs for adsorptive desulfurization of fuels. It was found that the REs tested show differing capacities for sulfur. Ce, the most extensively studied RE, has proven to be more effective then La, Nd, and Sm for BT and DBT adsorption in the presence of aromatics. DRIFTS studies were conducted and proved that all the RE adsorb via direct (S−M) σ bonds and π complexation. While Ce increased the possibility of sulfur adsorption via various configurations, the addition of Cu has played a key role in further increasing the adsorption capacity. In conjunction with ICP and XRF results, Rietveld refinement can be a very powerful tool to characterize important interatomic parameters of metal-modified zeolites. By use of this technique, it was shown that RE ions reside in SI′ and SII′ after calcination and Cu in SII. CuCeY and CuCeSAY performed better than the other exchanged zeolites tested for BT and DBT adsorption due in part to the amount of Cu atoms stabilized in SII. The combination of experimental and spectroscopic results coupled with Rietveld refinement has shown to be advantageous in the investigation of ADS as a viable desulfurization process. Density functional theory calculations on the REY and CuREY zeolites are ongoing, and this will be the objective of our future work.

■ ASSOCIATED CONTENT

Supporting Information

The Supporting Information is available free of charge at https://pubs.acs.org/doi/10.1021/acs.jpcc.1c01103.

Breakthrough capacity calculation; FTIR of free benzothiophene; refinement results and coordinates of REY and CuREY; Rietveld refinement diffraction patterns of LaY, NdY, SmY, CuLaY, CuNdY, and CuSmY; interatomic distances between cations and framework oxygens; 3D representation of Y zeolite and the corresponding coordination sites; chemical compo-

https://doi.org/10.1021/acs.jpcc.1c01103
J. Phys. Chem. C 2021, 125, 9107−9118

sition of REY and CuREY determined by XRF and Rietveld; H_2-TPR profile of monometallic Y and bimetallic CuREY (PDF)

AUTHOR INFORMATION

Corresponding Author

Julia A. Valla − *Department of Chemical and Biomolecular Engineering, University of Connecticut, Storrs, Connecticut 06269, United States;* orcid.org/0000-0002-4402-0818; Phone: +1 (860) 486 0583; Email: ioulia.valla@uconn.edu

Authors

Kevin X. Lee − *Department of Chemical and Biomolecular Engineering, University of Connecticut, Storrs, Connecticut 06269, United States*

Tyler B. Crowl − *Department of Chemical and Biomolecular Engineering, University of Connecticut, Storrs, Connecticut 06269, United States*

Henry J. Sokol − *Department of Chemical and Biomolecular Engineering, University of Connecticut, Storrs, Connecticut 06269, United States*

M. Daniela Morales-Acosta − *Institute of Materials Science, University of Connecticut, Storrs, Connecticut 06269, United States*

Complete contact information is available at: https://pubs.acs.org/10.1021/acs.jpcc.1c01103

Notes

The authors declare no competing financial interest.

ACKNOWLEDGMENTS

The NSF CAREER Award #1844767 and AMES program DE-EE0008302 are greatly acknowledged.

ABBREVIATIONS

TP, thiophene; BT, benzothiophene; DBT, dibenzothiophene; DMDBT, 4,6-dimethyldibenzothiophene; RE, rare earth; DRIFTS, diffuse reflectance infrared Fourier transform spectroscopy (DRIFTS); FTIR, Fourier transform infrared spectroscopy; XPS, X-ray photoelectron spectroscopy; XRF, X-ray fluorescence; XRD, X-ray diffraction.

REFERENCES

(1) EPA Sets Tier 3 Motor Vehicle Emission and Fuel Standards; EPA-420-F-14−009; U.S. Environmental Protection Agency, Office of Transportation and Air Quality, Washington, DC, 2014.

(2) Song, C. An Overview of New Approaches to Deep Desulfurization for Ultra-Clean Gasoline, Diesel Fuel and Jet Fuel. *Catal. Today* **2003**, *86*, 211−263.

(3) Velu, S.; Ma, X.; Song, C. Selective Adsorption for Removing Sulfur from Jet Fuel over Zeolite-Based Adsorbents. *Ind. Eng. Chem. Res.* **2003**, *42*, 5293−5304.

(4) Babich, I. V.; Moulijn, J. A. Science and Technology of Novel Processes for Deep Desulfurization of Oil Refinery Streams: A Review. *Fuel* **2003**, *82*, 607−631.

(5) Acar, C.; Dincer, I. The Potential Role of Hydrogen as a Sustainable Transportation Fuel to Combat Global Warming. *Int. J. Hydrogen Energy* **2020**, *45*, 3396−3406.

(6) Staffell, I.; Scamman, D.; Velazquez Abad, A.; Balcombe, P.; Dodds, P. E.; Ekins, P.; Shah, N.; Ward, K. R. The Role of Hydrogen and Fuel Cells in the Global Energy System. *Energy Environ. Sci.* **2019**, *12*, 463−491.

(7) Lee, K. X.; Valla, J. A. Adsorptive Desulfurization of Liquid Hydrocarbons Using Zeolite-Based Sorbents: A Comprehensive Review. *React. Chem. Eng.* **2019**, *4*, 1357−1386.

(8) Crandall, B. S.; Zhang, J.; Stavila, V.; Allendorf, M. D.; Li, Z. Desulfurization of Liquid Hydrocarbon Fuels with Microporous and Mesoporous Materials: Metal-Organic Frameworks, Zeolites, and Mesoporous Silicas. *Ind. Eng. Chem. Res.* **2019**, *58*, 19322−19352.

(9) Ma, X.; Velu, S.; Kim, J. H.; Song, C. Deep Desulfurization of Gasoline by Selective Adsorption over Solid Adsorbents and Impact of Analytical Methods on Ppm-Level Sulfur Quantification for Fuel Cell Applications. *Appl. Catal., B* **2005**, *56*, 137−147.

(10) Danmaliki, G. I.; Saleh, T. A.; Shamsuddeen, A. A. Response Surface Methodology Optimization of Adsorptive Desulfurization on Nickel/Activated Carbon. *Chem. Eng. J.* **2017**, *313*, 993−1003.

(11) Zhou, A.; Ma, X.; Song, C. Liquid-Phase Adsorption of Multi-Ring Thiophenic Sulfur Compounds on Carbon Materials with Different Surface Properties. *J. Phys. Chem. B* **2006**, *110*, 4699−4707.

(12) Kampouraki, Z. C.; Giannakoudakis, D. A.; Nair, V.; Bandegharaei, A. H.; Colmenares, J. C.; Deliyanni, E. A. Metal Organic Frameworks as Desulfurization Adsorbents of DBT and 4,6-DMDBT from Fuels. *Molecules* **2019**, *24*, 1−23.

(13) Ahmed, I.; Jhung, S. H. Adsorptive Desulfurization and Denitrogenation Using Metal-Organic Frameworks. *J. Hazard. Mater.* **2016**, *301*, 259−276.

(14) Zeng, Y.; Kaytakoglu, S.; Harrison, D. P. Reduced Cerium Oxide as an Efficient and Durable High Temperature Desulfurization Sorbent. *Chem. Eng. Sci.* **2000**, *55*, 4893−4900.

(15) Hussain, A. H. M. S.; Tatarchuk, B. J. Adsorptive Desulfurization of Jet and Diesel Fuels Using Ag/TiOx-Al2O3 and Ag/TiO x -SiO 2 Adsorbents. *Fuel* **2013**, *107*, 465−473.

(16) Wang, Y.; Yang, R. T.; Heinzel, J. M. Desulfurization of Jet Fuel by π-Complexation Adsorption with Metal Halides Supported on MCM-41 and SBA-15 Mesoporous Materials. *Chem. Eng. Sci.* **2008**, *63*, 356−365.

(17) Wang, Y.; Yang, R. T.; Heinzel, J. M. Desulfurization of Jet Fuel JP-5 Light Fraction by MCM-41 and SBA-15 Supported Cuprous Oxide for Fuel Cell Applications. *Ind. Eng. Chem. Res.* **2009**, *48*, 142−147.

(18) Hernández-Maldonado, A. J.; Yang, F. H.; Qi, G.; Yang, R. T. Desulfurization of Transportation Fuels by π-Complexation Sorbents: Cu(I)-, Ni(II)-, and Zn(II)-Zeolites. *Appl. Catal., B* **2005**, *56*, 111−126.

(19) Bhandari, V. M.; Ko, C. H.; Park, J. G.; Han, S. S.; Cho, S. H.; Kim, J. N. Desulfurization of Diesel Using Ion-Exchanged Zeolites. *Chem. Eng. Sci.* **2006**, *61*, 2599−2608.

(20) Li, K.; Valla, J.; Garcia-Martinez, J. Realizing the Commercial Potential of Hierarchical Zeolites: New Opportunities in Catalytic Cracking. *ChemCatChem* **2014**, *6*, 46−66.

(21) Van de Voorde, B.; Hezinová, M.; Lannoeye, J.; Vandekerkhove, A.; Marszalek, B.; Gil, B.; Beurroies, I.; Nachtigall, P.; De Vos, D. Adsorptive Desulfurization with CPO-27/MOF-74: An Experimental and Computational Investigation. *Phys. Chem. Chem. Phys.* **2015**, *17*, 10759−10766.

(22) Lee, K. X.; Tsilomelekis, G.; Valla, J. A. Removal of Benzothiophene and Dibenzothiophene from Hydrocarbon Fuels Using CuCe Mesoporous Y Zeolites in the Presence of Aromatics. *Appl. Catal., B* **2018**, *234*, 130−142.

(23) Wang, L.; Sun, B.; Yang, F. H.; Yang, R. T. Effects of Aromatics on Desulfurization of Liquid Fuel by π-Complexation and Carbon Adsorbents. *Chem. Eng. Sci.* **2012**, *73*, 208−217.

(24) Yang, R. T.; Hernández-Maldonado, A. J.; Yang, F. H. Desulfurization of Transportation Fuels with Zeolites under Ambient Conditions. *Science (Washington, DC, U. S.)* **2003**, *301*, 79−81.

(25) Shan, J. H.; Liu, X. Q.; Sun, L. B.; Cui, R. Cu-Ce Bimetal Ion-Exchanged Y Zeolites for Selective Adsorption of Thiophenic Sulfur. *Energy Fuels* **2008**, *22*, 3955−3959.

(26) Song, H.; Chang, Y.; Song, H. Deep Adsorptive Desulfurization over Cu, Ce Bimetal Ion-Exchanged Y-Typed Molecule Sieve. *Adsorption* **2016**, *22*, 139−150.

(27) Tian, F.; Shen, Q.; Fu, Z.; Wu, Y.; Jia, C. Enhanced Adsorption Desulfurization Performance over Hierarchically Structured Zeolite Y. *Fuel Process. Technol.* **2014**, *128*, 176−182.
(28) Lee, K. X.; Valla, J. A. Investigation of Metal-Exchanged Mesoporous Y Zeolites for the Adsorptive Desulfurization of Liquid Fuels. *Appl. Catal., B* **2017**, *201*, 359−369.
(29) Lee, K. X.; Wang, H.; Karakalos, S.; Tsilomelekis, G.; Valla, J. A. Adsorptive Desulfurization of 4,6-Dimethyldibenzothiophene on Bimetallic Mesoporous y Zeolites: Effects of Cu and Ce Composition and Configuration. *Ind. Eng. Chem. Res.* **2019**, *58*, 18301−18312.
(30) Nuntang, S.; Prasassarakich, P.; Ngamcharussrivichai, C. Comparative Study on Adsorptive Removal of Thiophenic Sulfurs over Y and USY Zeolites. *Ind. Eng. Chem. Res.* **2008**, *47*, 7405−7413.
(31) Subhan, F.; Liu, B. S.; Zhang, Y.; Li, X. G. High Desulfurization Characteristic of Lanthanum Loaded Mesoporous MCM-41 Sorbents for Diesel Fuel. *Fuel Process. Technol.* **2012**, *97*, 71−78.
(32) Verboekend, D.; Pérez-Ramírez, J. Design of Hierarchical Zeolite Catalysts by Desilication. *Catal. Sci. Technol.* **2011**, *1*, 879.
(33) García-Martínez, J.; Johnson, M.; Valla, J.; Li, K.; Ying, J. Y. Mesostructured Zeolite Y—High Hydrothermal Stability and Superior FCC Catalytic Performance. *Catal. Sci. Technol.* **2012**, *2*, 987.
(34) Marr, L. C.; Kirchstetter, T. W.; Harley, R. A.; Miguel, A. H.; Hering, S. V.; Hammond, S. K. Characterization of Polycyclic Aromatic Hydrocarbons in Motor Vehicle Fuels and Exhaust Emissions. *Environ. Sci. Technol.* **1999**, *33*, 3091−3099.
(35) Heavy-Duty Engine and Vehicle Standards and Highway Diesel Fuel Sulfur Control Requirements; EPA420-F-00-057; U.S. Environmental Protection Agency, Office of Transportation and Air Quality, Washington, DC, 2000.
(36) Zu, Y.; Guo, Z.; Zheng, J.; Hui, Y.; Wang, S.; Qin, Y.; Zhang, L.; Liu, H.; Gao, X.; Song, L. Investigation of Cu(I)-Y Zeolites with Different Cu/Al Ratios towards the Ultra-Deep Adsorption Desulfurization: Discrimination and Role of the Specific Adsorption Active Sites. *Chem. Eng. J.* **2020**, *380*, 122319.
(37) Toby, B. H.; Von Dreele, R. B. GSAS-II: The Genesis of a Modern Open-Source All Purpose Crystallography Software Package. *J. Appl. Crystallogr.* **2013**, *46*, 544−549.
(38) Baerlocher, C.; McCusker, L. Database of Zeolite Structures. http://www.iza-structure.org/databases (accessed 2017-06-01).
(39) Du, X.; Gao, X.; Zhang, H.; Li, X.; Liu, P. Effect of Cation Location on the Hydrothermal Stability of Rare Earth-Exchanged y Zeolites. *Catal. Commun.* **2013**, *35*, 17−22.
(40) Le Bail, A.; Duroy, H.; Fourquet, J. L. Ab-Initio Structure Determination of LiSbWO6 by X-Ray Powder Diffraction. *Mater. Res. Bull.* **1988**, *23*, 447−452.
(41) Lemos, F.; Ramôa Ribeiro, F.; Kern, M.; Giannetto, G.; Guisnet, M. Influence of Lanthanum Content of LaHY catalysts on Their Catalytic Properties. Comparison with CeHY Catalysts. *Appl. Catal.* **1988**, *39*, 227−237.
(42) Lemos, F.; Ramôa Ribeiro, F.; Kern, M.; Giannetto, G.; Guisnet, M. Influence of the Cerium Content of CeHY Catalysts on Their Physicochemical and Catalytic Properties. *Appl. Catal.* **1987**, *29*, 43−54.
(43) Song, H.; Cui, X.; Song, H.; Gao, H.; Li, F. Characteristic and Adsorption Desulfurization Performance of Ag-Ce Bimetal Ion-Exchanged Y Zeolite. *Ind. Eng. Chem. Res.* **2014**, *53*, 14552−14557.
(44) Song, C.; Ma, X. New Design Approaches to Ultra-Clean Diesel Fuels by Deep Desulfurization and Deep Dearomatization. *Appl. Catal., B* **2003**, *41*, 207−238.
(45) Tian, F.; Wu, W.; Jiang, Z.; Liang, C.; Yang, Y.; Ying, P.; Sun, X.; Cai, T.; Li, C. The Study of Thiophene Adsorption onto La(III)-Exchanged Zeolite NaY by FT-IR Spectroscopy. *J. Colloid Interface Sci.* **2006**, *301*, 395−401.
(46) García, C. L.; Lercher, J. A. Adsorption and Surface Reactions of Thiophene on ZSM5 Zeolites. *J. Phys. Chem.* **1992**, *96*, 2669−2675.
(47) Qiu, L.; Ying, F.; Jinyu, Z.; Nangui, H.; Lijun, L.; Xiuzhi, G.; Mudi, X.; Yibin, L.; Yanqiang, S.; Guangtong, X. Investigation on the Cation Location, Structure and Performances of Rare Earth-Exchanged Y Zeolite. *J. Rare Earths* **2017**, *35*, 658−666.
(48) Du, X.; Zhang, H.; Li, X.; Tan, Z.; Liu, H.; Gao, X. Cation Location and Migration in Lanthanum-Exchanged NaY Zeolite. *Chin. J. Catal.* **2013**, *34*, 1599−1607.
(49) Scherzer, J.; Bass, J. L. Structural Characterization of Hydrothermally Treated Lanthanum Y Zeolites. II. Infrared Spectra in the Hydroxyl Stretching Region and Acid Sites. *J. Phys. Chem.* **1975**, *79*, 1200−1205.
(50) Shy, D. S.; Chen, S. H.; Lievens, J.; Liu, S.-B.; Chao, K. J. Distribution of Cations in Lanthanum-Exchanged NaY Zeolites. *J. Chem. Soc., Faraday Trans.* **1991**, *87*, 2855−2859.
(51) Palomino, G. T.; Bordiga, S.; Zecchina, A.; Marra, G. L.; Lamberti, C. XRD, XAS, and IR Characterization of Copper-Exchanged Y Zeolite. *J. Phys. Chem. B* **2000**, *104*, 8641−8651.
(52) Egerton, T. A.; Stone, F. S. Adsorption of Carbon Monoxide by Zeolite Y Exchanged with Different Cations. *J. Chem. Soc., Faraday Trans. 1* **1973**, *69*, 22.
(53) Duan, L.; Gao, X.; Meng, X.; Zhang, H.; Wang, Q.; Qin, Y.; Zhang, X.; Song, L. Adsorption, Co-Adsorption, and Reactions of Sulfur Compounds, Aromatics, Olefins over Ce-Exchanged y Zeolite. *J. Phys. Chem. C* **2012**, *116*, 25748−25756.
(54) Zu, Y.; Qin, Y.; Gao, X.; Liu, H.; Zhang, X.; Zhang, J.; Song, L. Insight into the Correlation between the Adsorption-Transformation Behaviors of Methylthiophenes and the Active Sites of Zeolites Y. *Appl. Catal., B* **2017**, *203*, 96−107.
(55) Wang, Y.; Yang, F. H.; Yang, R. T.; Heinzel, J. M.; Nickens, A. D. Desulfurization of High-Sulfur Jet Fuel by π-Complexation with Copper and Palladium Halide Sorbents. *Ind. Eng. Chem. Res.* **2006**, *45*, 7649−7655.
(56) Zhang, L.; Qin, Y.; Zhang, X.; Gao, X.; Song, L. Further Findings on the Stabilization Mechanism among Modified y Zeolite with Different Rare Earth Ions. *Ind. Eng. Chem. Res.* **2019**, *58*, 14016−14025.
(57) Takahashi, A.; Yang, R. T.; Munson, C. L.; Chinn, D. Cu(I)-Y-Zeolite as a Superior Adsorbent for Diene/Olefin Separation. *Langmuir* **2001**, *17*, 8405−8413.

https://doi.org/10.1021/acs.jpcc.1c01103
J. Phys. Chem. C 2021, 125, 9107−9118